

# Theory of Two-Proton Radioactivity with Application to $^{19}\text{Mg}$ and $^{48}\text{Ni}$

L. V. Grigorenko,<sup>1,2</sup> R. C. Johnson,<sup>1</sup> I. G. Mukha,<sup>3</sup> I. J. Thompson,<sup>1</sup> and M. V. Zhukov<sup>4</sup>

<sup>1</sup>*Department of Physics, University of Surrey, Guildford GU2 7XH, United Kingdom*

<sup>2</sup>*Russian Research Center "The Kurchatov Institute," 123182 Moscow, Russia*

<sup>3</sup>*Institut für Kernphysik, Technische Universität, D-64289 Darmstadt, Germany*

<sup>4</sup>*Department of Physics, Chalmers University of Technology, S-41296 Göteborg, Sweden  
and Göteborg University, S-41296 Göteborg, Sweden*

(Received 24 March 2000)

We study the emission of two protons from nuclei where this is the only decay channel. A three-body model is developed. We compare the "diproton" model with the three-body calculations. We present exploratory studies of the  $^{19}\text{Mg}$  and  $^{48}\text{Ni}$  ground states, which are good candidates for two-proton radioactivity. The two-proton width for the  $^{17}\text{Ne}$   $3/2^-$  state is also estimated. Our calculations give substantially lower values for the width than predicted by the diproton model, but larger than from direct decay to the continuum.

PACS numbers: 23.50.+z, 21.10.Tg, 21.45.+v, 21.60.Gx

Emission of two protons from nuclear states has been studied since 1960 when two-proton radioactivity was predicted by Goldansky for nuclei beyond the proton dripline [1]. Two-proton decay may occur through three possible mechanisms: (i) sequential emission of protons via an intermediate state, (ii) simultaneous emission of protons, and (iii) "diproton emission," i.e., emission of a  $^2\text{He}$  cluster with very strong  $pp$  correlations. Experimentally only the first two mechanisms have been identified. The third case which is traditionally associated with the two-proton radioactivity [1–3] is unobserved yet. In this paper we consider two-proton emission in a more rigorous basis of a realistic three-body model. This model is suitable for treatment of a genuine three-particle nuclear decay mode (called "true three-body decay" in [1]), where resonances in the binary subsystems are located at higher energies than in the three-body system. This situation is in a sense similar to the "borromean" property of bound halo nuclei (e.g.,  $^6\text{He}$   $0^+$  and  $^{11}\text{Li}$   $3/2^-$  [4],  $^{17}\text{Ne}$   $1/2^-$  [5]). True three-body decay modes are known for several states in light nuclei, e.g.,  $^6\text{Be}$   $0^+$  [6],  $^9\text{Be}$   $5/2^-$  at 2.43 MeV [7],  $^{12}\text{C}$   $1^+$  at 15.11 MeV [8,9]. Nowadays, the prime candidates for the two-proton radioactivity are  $^{19}\text{Mg}$  and  $^{48}\text{Ni}$  [2], which are likely to be bound to single-proton decay but unbound to two-proton decay [10].

The traditional idea of diproton radioactivity is that, due to the pairing effect, two protons form a quasiparticle (diproton) under the Coulomb barrier and thus facilitate penetration. In more formal terms, we have a system with two valence protons in the same shell and coupled to  $J^\pi = 0^+$ . Conversion of the valence nucleons' wave function (WF) from single-particle coordinates (Fig. 1a) to the Jacobi "T" system (Fig. 1b) gives a large (for  $f_{7/2}$  nucleons about 46%) component with  $S_{pp} = 0$ ,  $l_x = l_y = 0$  ( $S_{pp}$  is the total spin of two protons;  $l_x$  and  $l_y$  are angular momenta conjugated to coordinates  $X$  and  $Y$ ). Dynamically this configuration is enhanced by pairing and

can be interpreted as a diproton in an  $s$  wave relative to the core.

Diproton models ordinarily use the two-body  $R$ -matrix expression for the width (e.g., [2]; in paper [3] a WKB model is applied, but essentially in the same way):

$$\Gamma = 2\gamma^2 P_{l=0}(E, 2Z_{\text{core}} r_c), \quad (1)$$

where  $P_{l=0}(E, 2Z_{\text{core}} r_c)$  is the penetrability for  $^2\text{He}$  with energy  $E$ .  $E$  is usually taken as a resonance energy above the two-proton threshold, so zero energy is left for the relative motion of two protons (e.g., [2,3,10]). Equation (1) then combines two incompatible things: penetration of a pointlike particle along some trajectory under the Coulomb barrier and zero energy of relative motion for the constituents of this particle. This last feature implies infinite size due to the uncertainty principle.

The original paper [1] is cautious about the diproton model. What Goldansky really finds as a genuine signal of two-proton emission is an "energy correlation between the two protons, during the two-proton decay, which leads to their energies being almost equal." According to [1,11], in the case of  $s$ -wave states, the diproton model and the model for simultaneous emission of two protons ("direct decay to continuum") give similar widths. This latter can

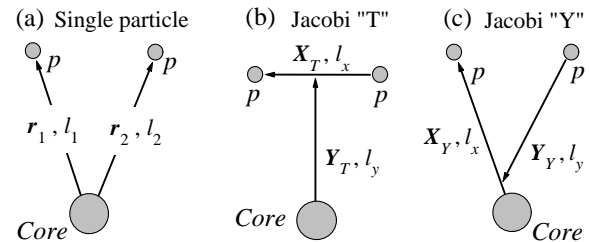


FIG. 1. Single-particle coordinate system (a), typical for a shell model. In the Jacobi "T" system (b), "diproton" and core are explicitly in configurations with definite angular momenta  $l_x$  and  $l_y$ . For a heavy core the Jacobi "Y" system (c) is close to the single-particle system (a).

be estimated from its maximal value, achieved for equal energies of protons:

$$\Gamma = 2\gamma^2[P_l(E/2, Z_{\text{core}}, r_c)]^2. \quad (2)$$

If  $l = 0$  is taken, the estimate based on Eq. (2) differs from that calculated by Eq. (1) by a factor close to unity. However, we are going to deal with nuclei where  $p$ - $f$  shells are occupied predominantly and an  $s$  wave is accessible only via small components. The uncertainties connected with the choice of  $l$  can be quite large, as was discussed in detail in [11] and will be seen in Fig. 2.

In the model described here we use the hyperspherical harmonic (HH) method [4]. In this method the absolute values of Jacobi coordinates  $X_i$  and  $Y_i$  for three particles (Figs. 1b and 1c) are expressed via hyperangle  $\theta_\rho$  and hyperradius  $\rho$ . Index  $i = \{T, Y\}$  selects the Jacobi system used: “T” or “Y.” In the “T” system  $\theta_\rho$  and  $\rho$  are given by

$$\theta_\rho = \arctan \left[ \sqrt{\frac{(A_{\text{core}}+2)}{4A_{\text{core}}}} \frac{X_T}{Y_T} \right],$$

$$\rho^2 = \frac{1}{2}X_T^2 + \frac{2A_{\text{core}}}{A_{\text{core}}+2}Y_T^2.$$

The WF in this method is expanded over the HHs

$$\Psi(X, Y) = \rho^{-5/2} \sum_{K\gamma} \chi_{K\gamma}(\rho) J_{K\gamma}(\Omega_\rho),$$

where  $J_{K\gamma}(\Omega_\rho)$  is the set of orthonormal basis functions complete on the hypersphere  $\Omega_\rho = \{\theta_\rho, \Omega_X, \Omega_Y\}$  of fixed radius  $\rho$ . The hypermoment  $K$  is a generalized angular momentum ( $K = l_x + l_y + 2n$ ;  $n = 0, 1, \dots$ ), while multiindex  $\gamma$  stand for the remaining quantum numbers:  $\gamma = \{L, l_x, l_y, S, S_{pp}\}$ . In the HH basis the variational

procedure reduces the Schrödinger equation to a set of coupled ordinary differential equations.

It is clearly impractical to solve the scattering problem to find the width of an extremely narrow state. We will model the narrow decaying state as a solution of

$$(\hat{H} - E + i\Gamma/2)\Psi^{(+)}(\rho, \Omega_\rho) = 0, \quad (3)$$

in a finite size domain with outgoing wave boundary conditions. Equation (3) is solved approximately using the idea that for a very narrow state the WF should be very close to a “box” WF  $\Psi_b$  in the internal region. The WF  $\Psi_b$  satisfies  $(\hat{H} - E_b)\Psi_b(\rho, \Omega_\rho) = 0$  for  $0 < \rho < \rho_b$  and vanishes for  $\rho \geq \rho_b$ . In practice the value  $\rho_b$  should be as large as possible, but still in the “classically forbidden” region. The WF  $\Psi_b$  is then used as a source term:

$$(\hat{H} - E_b)\Psi^{(+)}(\rho, \Omega_\rho) = -i(\Gamma/2)\Psi_b(\rho, \Omega_\rho). \quad (4)$$

This equation is solved subject to purely outgoing wave boundary conditions with arbitrary  $\Gamma$ . The actual width is then calculated from

$$\Gamma = \frac{1}{M} \frac{\text{Im} \int d\Omega_\rho \Psi^{(+)\dagger} \rho^{5/2} (d/d\rho) \rho^{5/2} \Psi^{(+)}|_{\rho_{\text{max}}}}{\int d\Omega_\rho \int_0^{\rho_{\text{max}}} d\rho \rho^5 |\Psi^{(+)}|^2}. \quad (5)$$

This exact formula is obtained by applying Green’s theorem to Eq. (3). Equation (5) has the simple physical meaning of the ratio of the current through the hypersphere of radius  $\rho_{\text{max}}$  to the number of particles inside it. The method was first tested in the two-body case giving a good agreement with conventional scattering calculations: the deviation is between 8% and 0.1% for widths in the range  $10^{-1} - 10^{-10}$  MeV, respectively.

The other approximations are connected with the three-body Coulomb interaction. It gives coupling potentials for the HH equations which decrease as  $\rho^{-1}$ , so the equations never decouple. One option is to switch off all the Coulomb potentials at a large radius  $\rho_{\text{max}} \gg \rho_b$ , so that solutions of Eq. (4) are matched to Coulomb functions

$$\chi_{K\gamma}^{(+)}(\rho_{\text{max}}) \propto G_{\mathcal{L}}(\eta_{K\gamma}, \kappa\rho_{\text{max}}) + iF_{\mathcal{L}}(\eta_{K\gamma}, \kappa\rho_{\text{max}}),$$

where  $\mathcal{L} = K + 3/2$  and the Sommerfeld parameter

$$\eta_{K\gamma} = 0. \quad (6)$$

The other option is to switch off all the nondiagonal Coulomb potentials beyond  $\rho_{\text{max}}$ . Then the  $\eta_{K\gamma}$  is

$$\eta_{K\gamma} = (\rho_{\text{max}}/v) V_{K\gamma, K\gamma}^{\text{Coul}}(\rho_{\text{max}}), \quad (7)$$

where  $v = \kappa/M$ ,  $\kappa = \sqrt{2ME}$ ,  $M$  is nucleon mass, and  $V_{K\gamma, K\gamma}^{\text{Coul}}$  is the Coulomb part of the HH potential [4].

In the calculations we use the  $s$ -wave  $pp$  potential  $V(R) = -31 \exp[-(R/1.8)^2]$ . For  ${}^6\text{Be}$  and  ${}^{17}\text{Ne}$  the core- $p$  potentials were taken from [4] and [5]. To diminish the ambiguity of calculations for  ${}^{19}\text{Mg}$  and  ${}^{48}\text{Ni}$  we used potentials which act only in the states with

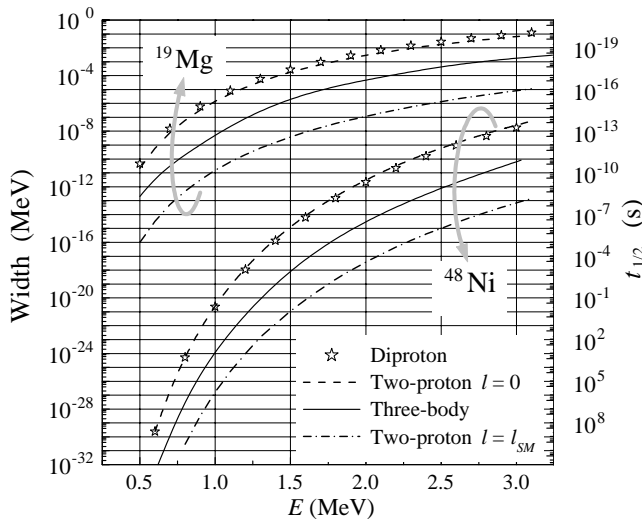


FIG. 2. Width as a function of resonance energy for  ${}^{19}\text{Mg}$  and  ${}^{48}\text{Ni}$ . Solid curves are calculated by Eq. (5). Stars, dashed, and dash-dotted curves correspond to estimates Eq. (1) (diproton), Eq. (2) (uncorrelated two protons) with  $l = 0$ , and  $l = l_{\text{SM}}$ . Channel radius is 3 fm for  ${}^{19}\text{Mg}$  and 4 fm for  ${}^{48}\text{Ni}$ ; the reduced width is approximated by the Wigner limit.

angular momentum  $l = l_{\text{SM}}$  of the dominant shell-model configuration occupied by the valence protons. The depth of this potential is controlled by the binding energy of the system. Woods-Saxon form factors were used, with diffuseness  $a = 0.65$  fm and radius  $r_0 = 1.2(A_{\text{core}} + 1)^{1/3}$  from systematics. At least, such a potential guarantees the population of the proper single particle states.

The results of calculations are shown in Table I and Fig. 2. The experimental width  $\Gamma = 92(6)$  keV of the  ${}^6\text{Be}$  g.s. is reproduced well. For all nuclei the widths calculated by Eq. (5) agree well for both choices [Eqs. (6) and (7) of boundary conditions, provided  $\rho_{\text{max}}$  is large enough (in calculations it was taken in a range 70–250 fm). It therefore appears that if the penetration through most of the barrier is accounted for dynamically, the choice of asymptotic state does not influence the width. In Fig. 2 we show the estimated widths for diproton decay, Eq. (1), and uncorrelated two-proton decay, Eq. (2), with different  $l$  values. The three-body calculations (see Fig. 2) lead to the widths which are substantially larger than widths for direct decay to the continuum from the dominant shell-model components ( $l_{\text{SM}} = 2$  for  ${}^{19}\text{Mg}$  and  $l_{\text{SM}} = 3$  for  ${}^{48}\text{Ni}$ ). At the same time the three-body widths are much smaller than the diproton widths, making it clear that although the three-body results include the  $pp$  correlations, these correlations are not strong enough to justify a pure diproton approach.

More realistic core- $p$  potentials for  ${}^{19}\text{Mg}$  and  ${}^{48}\text{Ni}$  (with  $LS$  forces from [12]) give results similar to those in Table I. For example, for  ${}^{48}\text{Ni}$  at  $E = 1.12$  MeV we obtain  $\Gamma_{\text{Coul}} = 4.0(0.5) \times 10^{-23}$  MeV.

Blank *et al.* [10] use the diproton model and a limit for the width to put a limit on the separation energy  $Q_{2p} < 1.5$  MeV for  ${}^{48}\text{Ni}$ . The predictions of the three-body model, applied in the same way, shift this limit to  $Q_{2p} < 2$  MeV. The calculated two-proton width for the  ${}^{17}\text{Ne}$   $3.2^-$  state is found to be very low compared to the total width  $\Gamma = 1.3 \times 10^{-8}$  MeV [13] which is presumably governed by electromagnetic transitions.

The WF densities  $|\Psi^{(+)}|^2$  on the  $XY$  plane in the “T” system are shown in Figs. 3a and 3c. The densities show

three- and four-peak correlations typical for  $d$ - and  $f$ -shell population. To demonstrate the barrier penetration process, we also calculate the density of the hyperradial current

$$J(X, Y) = \text{Im} \int d\Omega_X d\Omega_Y \Psi^{(+)\dagger} \rho^{5/2} \frac{d}{Md\rho} \rho^{5/2} \Psi^{(+)} \quad (8)$$

In the internal region the penetration flow patterns are very complicated (Figs. 3b and 3d). At small distances they follow the correlations typical for the internal region. Under the barrier these correlations are washed out and the “diproton path” close to the  $Y$  axis becomes important. A smooth hyperangular distribution without nodes means that the dominant component has  $K = 0$ , where both protons have  $l = 0$  relative to the core and hence escape the barrier more easily. Finally, the classically allowed region is achieved, after which the protons fly more or less freely (straight “tails” with constant value of  $J$  in Figs. 3b and 3d). For different energies this quasifree behavior happens at hyperradii which are inversely proportional to the energy. The direction of the tail is practically independent of energy, with mean velocity along the  $Y$  axis slightly larger than mean velocity along  $X$ .

We can get additional insight into the importance of pairing by simulating the uncorrelated two-proton case. The interaction in the  $pp$  channel can be switched off and core- $p$  interaction is adjusted to give the same resonance energy. Figure 3e shows the example of such “direct decay to the continuum” for  ${}^{48}\text{Ni}$ . The correlations of the nuclear interior survive to very large distances. The probability of decay is now very low, because in this case the protons are in an  $f$ -wave relative to the core, inhibiting the penetration. For example, for  $E = 1.12$  MeV in  ${}^{48}\text{Ni}$ ,  $\Gamma_{\text{Coul}} = 2.1 \times 10^{-26}$  MeV, which is close to the  $R$  matrix estimate,  $\Gamma = 9.4 \times 10^{-26}$  MeV, with two  $f$ -wave protons (Fig. 2). The  $pp$  interaction enhances the mixing of configurations and gives the system the opportunity to escape via lower angular momenta states. However, one can see in Figs. 3b and 3d that the three- and four-peaked internal correlations (Figs. 3a and 3c) disappear only at distances  $Y$  of about 15–20 fm. Hence for most of the path the two protons reside under a much higher barrier than is assumed by the simple model with a diproton in an  $s$ -wave state.

It should be noted that both with and without pairing, the hyperangular spread of the decay “tail” is very narrow in the “Y” coordinate system (Fig. 3f shows one plot as they are all rather similar). This means that the protons’ energies relative to the core are close to each other irrespective of the correlation in the  $pp$  channel. This agrees well with the prediction of Goldansky [1].

To conclude, a quantitative three-body model is developed to study the process of two-proton emission. The results show that truncation of the Coulomb potential at large distances does not lead to uncertainties in the energy and width or in the WF in the “internal” domain.

TABLE I. Two proton decay widths. Values  $\Gamma_{\text{PW}}$  and  $\Gamma_{\text{Coul}}$  are calculated using approximations of Eqs. (6) and (7), respectively. Values in parentheses are estimates of the uncertainties of the theoretical model.

State	$E$ , MeV	$\Gamma_{\text{PW}}$ , MeV	$\Gamma_{\text{Coul}}$ , MeV
${}^6\text{Be}$ , $0^+$	1.370	0.095(0.01)	0.09(0.01)
${}^{17}\text{Ne}$ , $3/2^-$	0.344	$1.0(0.4) \times 10^{-15}$	$1.4(0.3) \times 10^{-15}$
${}^{19}\text{Mg}$ , $0^+$	0.548	$8.0(3.7) \times 10^{-13}$	$8.7(1.4) \times 10^{-13}$
	0.838	$3.8(0.8) \times 10^{-10}$	$3.7(0.2) \times 10^{-10}$
	1.408	$8.1(0.8) \times 10^{-7}$	$8.2(0.2) \times 10^{-7}$
${}^{48}\text{Ni}$ , $0^+$	0.762	$4.0(3.0) \times 10^{-29}$	$4.0(1.0) \times 10^{-29}$
	1.120	$6.1(0.7) \times 10^{-23}$	$5.8(0.3) \times 10^{-23}$
	2.093	$9.6(1.6) \times 10^{-15}$	$9.5(0.3) \times 10^{-15}$
	3.030	$9.0(0.2) \times 10^{-11}$	$8.16(0.02) \times 10^{-11}$

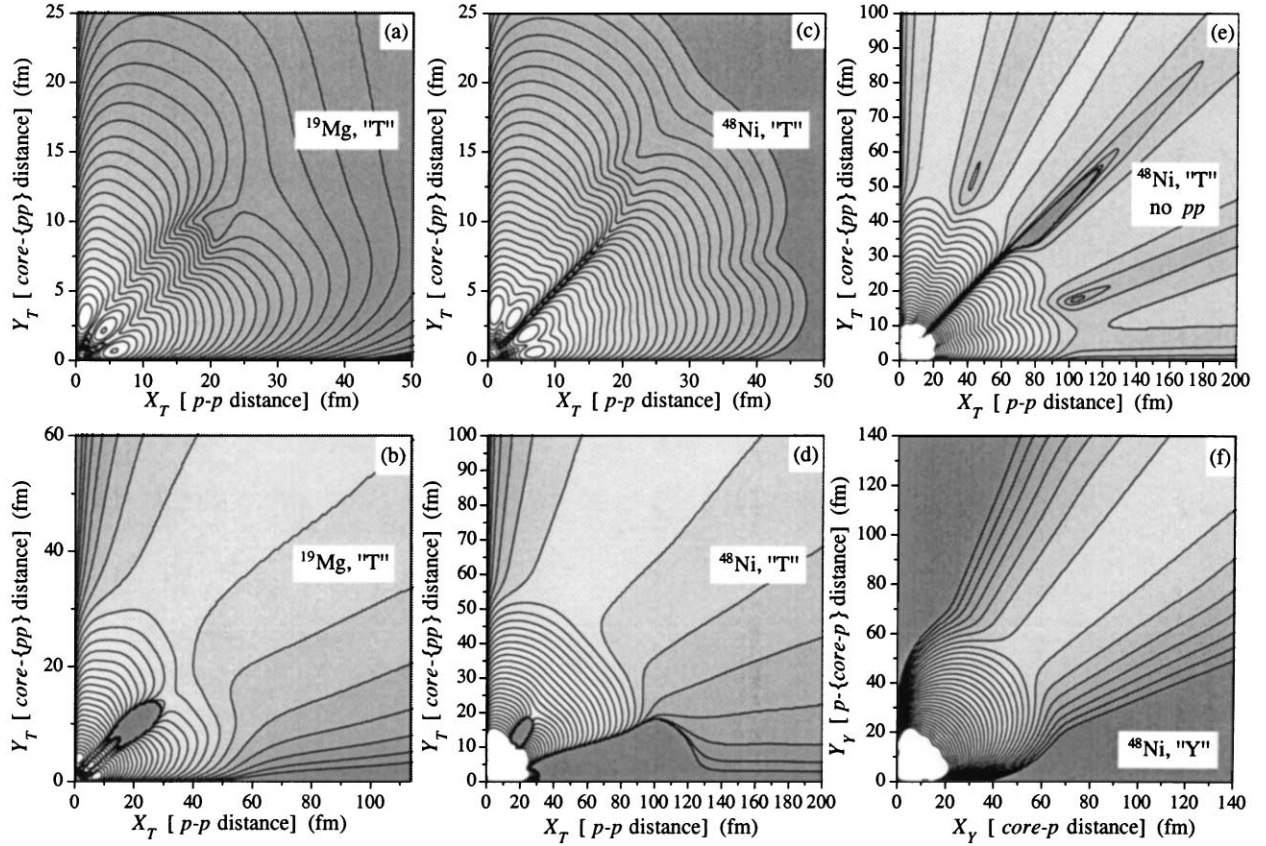


FIG. 3.  $^{19}\text{Mg}$ : WF density  $|\Psi^{(+)}|^2$  (a) and current density  $J(X,Y)$  (b) at  $E = 0.90$  MeV in the “T” system.  $^{48}\text{Ni}$ : WF density (c) and current density (d) at  $E = 1.12$  MeV in the “T” system. (e) shows the same as (d), but without pairing. (f) shows the same as (d),(e), but in the “Y” system. The scale is three (a),(b) and two (c)–(f) contours per order of magnitude. The dark regions in (b),(d) at small  $\rho$  values stand for the negative current “backflow” invisible in the logarithmic plot.

However, other interesting observables (e.g., momentum distributions) need further investigation. The results of the calculations predict much lower widths for two-proton emission than the widely used diproton model, where the emission of two protons with zero relative energy is assumed. For a given decay width, this increases any fitted decay energy: for  $^{48}\text{Ni}$  this shifts the limit from  $Q_{2p} < 1.5$  MeV [10] to  $Q_{2p} < 2$  MeV. The calculated two-proton width for the  $^{17}\text{Ne}$   $3/2^-$  state is negligible compared to the electromagnetic decay width. The  $pp$  pairing was found to be very important for penetration, but the penetration pattern is complicated and involves various paths which cannot be accounted for properly in a diproton model. The correlations which exist in the interior of the nucleus are drastically smoothed by the proton pairing and Coulomb interactions before the asymptotic region is reached.

The authors thank B. V. Danilin and N. B. Shul’gina for valuable discussions. L. V. G. is grateful for support from Royal Swedish Academy of Science and the hospitality of Chalmers University of Technology, where part of this work was done. I. G. M. is supported by the German Federal Minister for Education and Research (BMBF) under

Contract No. 06 DA 820. We acknowledge the support of EPSRC Grant No. GR/J95867 and RFBR Grant No. 00-15-96590.

- 
- [1] V. I. Goldansky, Nucl. Phys. **19**, 482 (1960).
  - [2] B. A. Brown, Phys. Rev. C **43**, R1513 (1991).
  - [3] W. Nazarewicz *et al.*, Phys. Rev. C **53**, 740 (1996).
  - [4] M. V. Zhukov *et al.*, Phys. Rep. **231**, 153 (1993).
  - [5] M. V. Zhukov and I. J. Thompson, Phys. Rev. C **52**, 3505 (1995).
  - [6] B. V. Danilin *et al.*, Sov. J. Nucl. Phys. **46**, 225 (1987); O. V. Bochkarev *et al.*, Nucl. Phys. **A505**, 215 (1989).
  - [7] O. V. Bochkarev *et al.*, Sov. J. Nucl. Phys. **52**, 1525 (1990); G. Nyman *et al.*, Nucl. Phys. **A510**, 189 (1990).
  - [8] D. P. Balamuth, R. W. Zurmühle, and S. L. Tabor, Phys. Rev. C **10**, 975 (1974).
  - [9] A. A. Korshennikov, Sov. J. Nucl. Phys. **52**, 827 (1990).
  - [10] B. Blank *et al.*, Phys. Rev. Lett. **84**, 1116 (2000).
  - [11] J. Jänecke, Nucl. Phys. **61**, 326 (1965).
  - [12] F. D. Becchetti and G. W. Greenlees, Phys. Rev. **182**, 1190 (1969).
  - [13] M. J. Chromik *et al.*, Phys. Rev. C **55**, 1676 (1997).